EGYPTIAN ACADEMIC JOURNAL OF

BIOLOGICAL SCIENCES

HISTOLOGY & HISTOCHEMISTRY

D

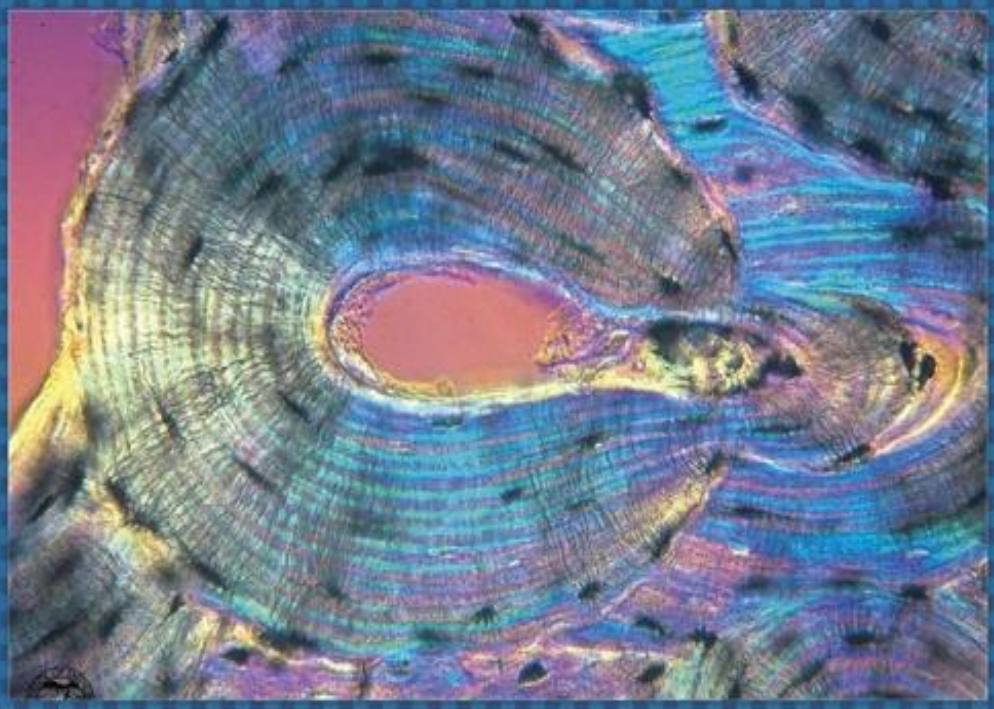

ISSN
2090-0775

WWW.EAJBS.EG.NET

Vol. 15 No. 1 (2023)

Citation: Egypt. *Acad. J. Biolog. Sci. (D-Histology and histochemistry) Vol.15(1) pp17-38(2022)*
DOI: 10.21608/EAJBSD.2023.282307

Egypt. Acad. J. Biolog. Sci., 15(1): 17-38 (2023)

Egyptian Academic Journal of Biological Sciences
D. Histology & Histochemistry
ISSN 2090 – 0775
http://eajbsd.journals.ekb.eg

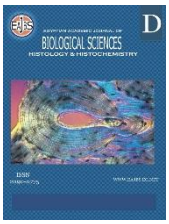

Histological and Immunohistochemical Study of Tartrazine Effect on The Adult Albino Rat Parotid Gland and The Possible Protective Role of Omega-3 Fatty Acids.

Hala Mohamed Hassanin and Merry BK. Shenouda
Human Anatomy and Embryology Department, Faculty of Medicine, Assiut University, Egypt
E.Email : halahasenien@aun.edu.eg - merrybeniamen@aun.edu.eg

ARTICLE INFO
Article History
Received:24/12/2022
Accepted:25/1/2023
Available:29/1/2023

***Keywords*:**
Parotid Gland, Tartrazine, Caspase-3, Omega-3-Fatty Acids, Collagen fibers.

ABSTRACT

Introduction: Tartrazine is a broadly used food additive. It can induce several adverse effects on different body organs. Omega-3 fatty acids have a documented antioxidant, anti-apoptotic and anti-inflammatory effects. **Aim of the work:** To study the induced histological changes by tartrazine in the parotid gland and to investigate the protective action of omega-3-fatty acids against these changes.**Material and Methods:** Twenty-one adult male albino rats were divided into 3 groups; Group I (control group), Group II (tartrazine-treated group) received tartrazine daily at a dose of 320 mg/kg body weight orally and Group III (tartrazine and omega-3 treated group) received omega-3 daily at a dose of 300 mg/kg body weight orally in addition to tartrazine in the same dose in group II. The treatment continued for four weeks. Parotid gland specimens were processed for light microscopic examination using Hematoxylin and Eosin, Sirius red stains and caspase-3 immunostaining in addition to electron microscopic examination**. Results**: Parotid acini in tartrazine-treated group showed a histological deterioration in the form of darkly stained nuclei and cytoplasmic vacuolations. Statistically, area % of both collagen fibers staining and caspase-3 immunostaining increased significantly in comparison to the control group. Ultrastructurally, irregular nuclei, electron-lucent granules dominance and dilated rough endoplasmic reticulum were detected in the acinar cells of tartrazine-treated group in addition to degenerative changes in ductal epithelium. Treatment with omega-3 improved the structure of the parotid gland as detected by both histological and morphometric studies.

Conclusion Omega-3 treatment ameliorated the structural effects of tartrazine on the parotid gland.

INTRODUCTION

The major salivary glands in human comprise the parotid, sublingual, and submandibular glands. The parotid gland is serous in both human and rodents (Roa & Del Sol, 2019). In rodents, the parotid gland is located behind and below the ear, caudally bordering the submandibular gland (Amano *et al.*, 2012). Parotid gland consists of the parenchyma (glandular secretory tissue) and the stroma (the supporting connective tissue). The parenchyma comprises of secretory acini, intercalated ducts, striated ducts and collecting ducts, that join to form the main duct (Harrison, 2021).

It produces a serous secretion that contributes to over 50% of the total body saliva (Humphrey and Williamson, 2001). The saliva has several functions. It facilitates tasting, mastication, swallowing maintaining a moist oral mucosa, and removal of micro-organisms, desquamated epithelial cells, leucocytes, and food debris. Salivary amylase is involved in digestion of starch. It acts as a buffer to protect oral, pharyngeal, and esophageal mucosae from orally ingested acid. Moreover, the saliva contains many antiviral, antibacterial and antifungal agents (Dawes *et al.,* 2015)

The excess consumption of food additives or color is increasingly becoming an important subject as it alters the body's defense mechanism which leads to damage to the tissues and organs (Iheanyichukwu *et al.,* 2021). Azo dyes are the most popular synthetic dye in the food industry (Akkapinyo et al., 2021). The azo dye molecule can be cleaved into aromatic amines, which are known to be carcinogens and mutagens (Pogacean *et al.,* 2018). Tartrazine is a synthetic azo dye primarily used as a food colorant that on application provides a yellow to orange color. It is known by other names such as E102 and Yellow 5 or C.I. 19140 and was certified as a colorant by FDA for its use in drugs, food and cosmetics (Bhatt et al., 2018). It is one of the most widely used synthetic food dyes in the food industry and mainly found in drinks, fruit juices, chocolates, cookies, chewing gum, jam, candies, ice cream, sauces and mustard (Zingue *et al.,* 2021).

Tartrazine is involved in allergies, mutagenic and genotoxicity as well as neurobehavioral disorders (Engel *et al.,* 2015). Its oxidative damage was attributed to the production of sulphanilc acid as a metabolite (Bhatt *et al.,* 2018). It has a genotoxic effect due to its direct contact with the nuclear DNA that causes DNA damage (Khayyat *et al.,* 2017). Omega-3 polyunsaturated fatty acid and its metabolites, eicosapentaenoic acid (EPA) and docosahexaenoic acid (DHA), have many biological effects, including immunoregulatory, antioxidant, anti-inflammatory, anti-apoptotic and antitumor activities (Meital *et al.,* 2019). The main sources of omega-3 fatty acids include plants, marine animals and microorganisms. Plant seeds rich in omega-3 include flaxseed, chia seed and perilla seed (Abad & Shahidi, 2020). Flesh of fatty fish such as mackerel, and salmon, the liver of white lean fish such as cod are considered rich marine animal sources of omega-3 fatty acids (Unda, 2020).

Considering the oxidative damage of tartrazine in various body organs besides their extensive use to color food products, attention has been focused on the application of the active antioxidants. The protective role of omega-3 fatty acids against tartrazine induced oxidative stress was not previously fully investigated. Therefore, the present study was performed to investigate the consequent effects of tartrazine on histological structure of the parotid glands of albino rats and to study the possible protective role of omega-3 fatty acids against these effects.

MATERIALS AND METHODS

1. Chemicals:

a- Tartrazine ($C_{16}H_9N_4\ Na_3O_9S_2$). It was obtained from GFS chemicals – India, in the form of orange powder.

b- Omega-3 fatty acids: It was obtained from Solarbio life sciences Co. It was provided as an oily solution with a concentration of 1000 mg/5 ml fish oil.

2. Animals and Experiment Design and Treatment Regimen:

In this study twenty-one adult male albino rats; aged three months, weighing (220– 250 g) were used. They were obtained from the Animal House of

Faculty of Medicine, Assiut University. The rats were housed in cages in a temperature that was maintained at 23 ±2ºC, humidity (60 ± 10%) and under a 12 h light/12 h dark cycle. They were given free access to food and tap water ad libitum. They were acclimatized to the laboratory conditions for 15 days before being experimented. The rats were randomly assigned into three equal groups, 7 rats each. Group I (control group) did not receive any medications. Group II (tartrazine-treated group) in which rats received 320 mg/kg body weight tartrazine dissolved in 1 ml distilled water once a day by a gastric tube for 4 weeks. The dose represents 5% of LD_{50} of tartrazine in rat which is 6375 mg/kg body weight (Boussada et al., 2017). Group III (tartrazine and omega-3 treated group) were received omega -3 at a dose of 300 mg/ kg body weight by a gastric tube once a day (Elaziz & Laag, 2018) in addition to tartrazine administration at the same dose in group II for four weeks. All experimental procedures were in accordance with International Guidelines for the Care and Use of Laboratory Animals and were approved by the Ethical Committee at the Faculty of medicine, Assiut University. Egypt (IRB17300848).

At the end of the experiment, the animals were anaesthetized with inhalation of ether, and the heart was perfused with saline solution. After being sacrificed, the parotid salivary glands were identified by their location below the ear on the lateral side of the submandibular salivary glands and were dissected carefully and removed in one piece. The right glands were used for histological and immunohistochemical studies. The left parotid salivary glands were used for transmission electron microscopic study.

I- Histological Study:

1-Light Microscopic Study:

Specimens were immediately fixed in 10% neutral formalin for 48 hours and then rinsed in distilled water. They were dehydrated in ascending grades of ethyl alcohol and embedded in paraffin. The sections were cut and processed for:

a-Hematoxylin and Eosin staining to study the cytoarchitecture of the parotid gland (Bancroft & Layton, 2019)

b-Sirius red staining to examine the extent of fibrosis, as it specifically stains collagen fibers (Junqueira et al., 1979).

c-Immunohistochemical staining:

Sections of 4 µm thickness were placed on positive charged slides. The sections were then deparaffinized. The endogenous peroxidase activity was blocked using 3% hydrogen peroxide (H_2O_2) in PBS for 30 min. Microwaving of the sections was done for antigen retrieval by 0.01 M sodium citrate buffer (pH 6.0). The sections were rinsed in PBS, blocked with normal goat serum and then incubation with the primary antibody rabbit anti-cleaved caspase- 3 monoclonal antibody (diluted 1:100; Cell Signaling Technology, Boston, MA, USA) was done overnight. The slides were then rinsed and incubated with secondary biotinylated goat anti-mouse (diluted 1:150 in PBS; Zymed, San Francisco, CA, USA), for 3 hours at room temperature. Sections were washed in PBS and incubated with streptavidin-labelled peroxidase complex (diluted 1:150 in PBS; Zymed) for 3 hours at room temperature. The reaction was visualized with 0.6 mg/ml 3,3-diaminobenzidine tetrahydrochloride (DAB, Sigma–Aldrich) dissolved in PBS. The sections were counterstained with Mayer's hematoxylin. Finally, they were dehydrated, mounted, examined, and photographed (Sanderson *et al.,* 2019).

2-Transmission Electron Microscopic Study:

Specimens of the parotid gland were cut into small pieces (1 mm^3) fixed in 2.5% glutaraldehyde in phosphate buffer (pH 7.4). They then were fixed for 1h in 1% osmium tetroxide in same

buffer. Then, dehydration and embedding in epoxy resin was carried out. Semithin sections (0.5 µm) were cut, stained by toluidine blue stain, examined, and photographed. Ultrathin sections (80-90 nm) were cut using the ultramicrotome (Leica, Germany) and mounted on copper grids and stained with uranyl acetate and lead citrate (Woods & Stirling, 2019). They were examined and photographed by Jeol-JEM-100 CXII transmission electron microscope (Tokyo, Japan) at the electron microscopy unit in Assiut University.

II-Morphometric Study:

Sirius red stained sections and caspase-3 immunostained sections were photographed using Olympus digital camera (DP27) installed on Olympus microscope with 0.5x photo adaptor, using objective lens x 40 (TX 31 Philippines). The resultant images were morphometrically analyzed using ImageJ software (Java 8. 1.6.0. 2017. NIH, USA)**.** Dimensions were converted from pixels to micrometer by the software. Five different non-overlapping fields at a magnification of x400 were randomly chosen from five different sections of each animal from each group. The following parameters were measured:

1-The Area Percentage (%) Of Collagen Fibers Staining:

The RGB (Red, Green, Blue) threshold was used to identify the red stained areas of collagen fibers which was quantified as area percentage to the total area in a standard measuring frame (Fortea *et al.*, 2018).

2-The Area Percentage (%) of Caspase-3 Immunostaining:

Caspase-3 immunostaining was quantified as area percentage. The positive staining area was quantified with Image J software and the data were expressed as percentage of positive staining area to the total area in a standard measuring frame. The areas displaying brown color were selected for measurement regardless of the intensity (Galal et al., 2019).

III-Statistical Analysis:

The obtained data were statistically analyzed. Mean values and standard error mean (SEM) were represented. Statistical analysis was made with SPSS 19.0 software (Statistical Package for Scientific Studies, SPSS, Inc., Chicago, IL, USA). One-way analysis of variance (ANOVA) and post-hoc multiple comparison with Tukey's test was used to verify the differences among groups. The sitting of the significance level was at $P < 0.05$.

RESULTS

I-Histological Results:

A-Light Microscopic Results:

1-Haematoxylin and Eosin Staining:

Examination of the control group revealed the normal histological structure. The parotid gland was divided into lobes and lobules by thin delicate connective tissue septa. Its parenchyma consisted of serous acini and ducts. The excretory (interlobular) duct appeared with a pseudostratified columnar epithelium (Fig.1a). The acini lining cells were pyramidal in shape with rounded basally located nuclei and basophilic cytoplasm at the base and eosinophilic toward the apex. The intercalated duct was located and compressed among the acini and lined by low cuboidal cells, with central nuclei. The striated ducts appeared lined with columnar epithelial cells with acidophilic cytoplasm that showed basal striations and central spherical vesicular nuclei (Fig. 1b).

In the tartrazine-treated group (Group II) thickened connective tissue septa was observed between the lobules in addition to the presence of homogenous acidophilic material and interstitial cellular infiltration. The interlobular ducts appeared with disorganized cellular lining (Fig. 2a). The cellular lining of the interlobular ducts appeared with vacuolated cytoplasm and pyknotic nuclei. Congested periductal vessels

were observed. The acinar cells exhibited deeply stained nuclei, vacuolations of their cytoplasm. Red blood cells extravasation was noticed in between the acini (Fig. 2b). The intercalated ducts showed flattened disorganized cellular lining. The lining cells of the striated duct showed loss of striations in addition to vacuolated cytoplasm and pyknotic nuclei with shedding of their epithelial lining into the lumen (Fig. 2c)

In the tartrazine and omega-3 treated group, the parotid gland parenchyma consisted of lobes and lobules separated by thin connective tissue septa (Fig. 3a). The acini of the parotid gland appeared with pyramidal cellular lining with rounded basal nuclei. The intercalated, striated, and interlobular ducts appeared similar to the control group (Figs. 3a and 3b)

2-Sirius Red Staining:

Examination of Sirius-red stained sections in the control group revealed fine collagen fibers in between lobules and in relation to the ducts and surrounding the acini (Fig. 4a). In the tartrazine-treated group dense collagen fibers in the connective tissue septa and surrounding interlobular ducts and blood vessels was detected (Fig. 4b). In the tartrazine and omega-3 treated group, a moderate amount of collagen fibers appeared surrounding ducts and blood vessels (Fig. 4c).

3-Toluidine Blue Staining:

Examination of semithin sections of the parotid gland in the control group revealed an intact parenchyma that appeared formed of closely packed serous acini that were lined by pyramidal cells with basal rounded vesicular nuclei with prominent nucleoli. The cytoplasm appeared packed with granules of different densities. The intercalated ducts appeared compressed between the acini with low cuboidal cellular lining with oval vesicular nuclei. Striated ducts lining cells were columnar and showed a basally striated cytoplasm and central rounded vesicular nuclei. They were surrounded by myoepithelial cells (Fig. 5a). The interlobular duct appeared with a pseudostratified lining and was surrounded by myoepithelial cells (Fig. 5b).

In the tartrazine-treated group the parotid gland showed that serous acini lining cells appeared with darkly stained irregular nuclei. The cytoplasm showed many vacuolations in addition to an apparent decrease in the densely stained granules with an accumulation of lightly stained granules. Disorganized acini could be observed. The Intercalated ducts appeared with a discontinuity in the epithelial lining with most of cellular lining appeared with a vacuolated cytoplasm. The lining of the striated ducts showed a disruption and pyknotic nuclei (Fig. 5c). The interlobular ducts exhibited lining cells with a vacuolated cytoplasm and pyknotic nuclei in addition to exfoliated cells in its lumen. Congested blood vessels were observed. Some acini showed dilated intercellular spaces (Fig. 5d)

In the tartrazine and omega-3 treated group, most of the acini appeared with apparently normal pyramidal cells. The cells had rounded basal nuclei and cytoplasm rich in granules with different densities. Intercalated, striated and interlobular ducts appeared with a nearly normal lining. Some congested blood vessels were observed (Figs. 5e and 5f).

4-Immunohistochemical Staining:

The examination of caspase -3 immunostaining in the control group showed that the acinar cells and cells lining the ducts showed a mild immunostaining (Fig. 6a) while in the tartrazine-treated group, strong nuclear and cytoplasmic immune reaction of caspase-3 was observed in both the acinar and the lining of the ducts (Fig. 6b). The rats treated with tartrazine in combination with omega-3 showed a moderate immune reaction for caspase-3

in the acinar cells and in the cells lining the ducts with most of nuclei showed a negative reaction (Fig. 6c).

B- Electron Microscopic Results:

In the control group, the acinar cells were characterized by basally located rounded euchromatic nuclei with well-defined nucleoli, abundant rough endoplasmic reticulum around the nucleus arranged in parallel cisternae. Intercellular junctional complexes and intercellular canaliculi were observed (Fig.7a). A great number of spherical secretory granules of different electron-density and well-defined membrane in the supranuclear region of cytoplasm were observed with some granules are of high electron-dense content, some were of moderate homogeneous electron-dense content and other granules were of a low density. In the intercellular canaliculi, the adjacent cells interdigitate by infoldings of the lateral plasma membrane (Fig.7b). Examination of the lining cells of the striated duct revealed that they were columnar cells that showed rounded euchromatic central nuclei with regular nuclear membrane. The apical cytoplasm showed small secretory granules. Mitochondria were distributed in the basal and middle parts of the cell. Junctional complexes were observed near the lumen in addition to apical microvilli (Fig.7c).

In the tartrazine -treated group, the acinar cells appeared with irregular heterochromatic nuclei. Most of the secretory granules appeared electron lucent or of low electron density in the supranuclear region. In addition, the cytoplasm showed many vacuoles. The intercellular canaliculi were dilated with absence of the junctional complexes (Fig. 8a). Some cells showed an indented nuclear membrane. Fused outlines of many granules were observed (Fig. 8b). Dilated perinuclear cisterna and irregular cystic dilation of rough endoplasmic reticulum cisternae were noticed (Fig.8c). The lining cells of the striated duct showed a condensed central nucleus, rarified cytoplasm that showed mitochondria with destructed cristae and absence of microvilli (Fig. 8d).

In the tartrazine and omega-3 -treated group, the ultrastructural examination revealed that the acinar cells appeared similar to the control acinar cells with rounded basal euchromatic nucleus and many highly electron dense granules and moderately electron-dense secretory granules with apparently normal rough endoplasmic reticulum (Figs. 9a and 9b). The lining cells of the striated ducts showed a central rounded nucleus, apical small secretory granules with mitochondria distributed in the middle and basal parts of the cell. Microvilli were observed (Fig. 9c).

C-Morphometric Results:

The area percentage of collagen fibers staining in the parotid gland of the tartrazine treated group significantly increased when compared with the control group. However, in the tartrazine and omega-3 treated group, collagen fibers staining showed a significant decrease as compared with the tartrazine-treated group (Graph 1 and Table 1).

The area percentage of caspase-3 immunstaining in the parotid gland of the tartrazine treated group showed a statistically significant increase when compared to the control group. The caspase-3 immunostaining was significantly decreased in the tartrazine and omega-3 treated group in comparison to the tartrazine treated group. (Graph 2 and Table 1).

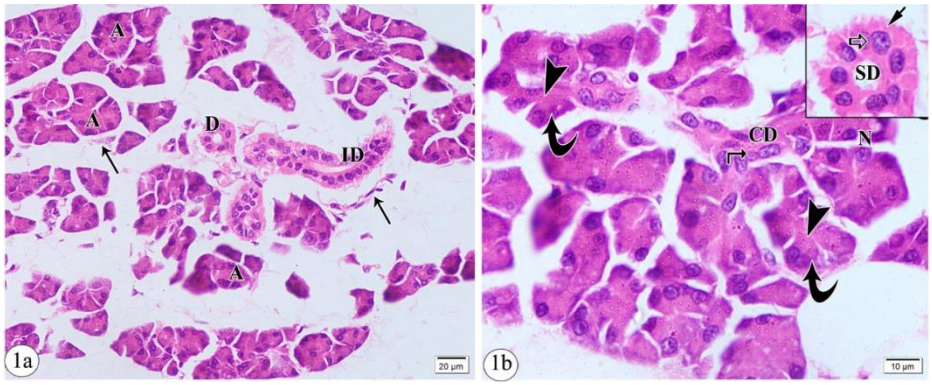

Fig. 1: Photomicrographs of H&E-stained sections in the parotid gland in the control group showing: **Fig.1a:** The gland consists of lobules separated by thin connective tissue septa (thin arrow). The parenchyma shows serous acini (A) and ducts (D). Interlobular duct appears in between the lobules and is lined by pseudostratified epithelium (ID) **(H & E X400). Fig.1b:** The acini lining cells are pyramidal in shape with rounded basally located nuclei (N) and the cytoplasm is basophilic basally (curved arrow) and eosinophilic toward the apex (arrowhead). The Intercalated duct (CD) is seen among the acini and lined by low cuboidal cells, with central nuclei (kinked arrow). **Inset:** A striated duct (SD) with a columnar cellular lining, an acidophilic cytoplasm, basal striations (short arrow) and central spherical vesicular nuclei (thick arrow) **(H & E X1000).**

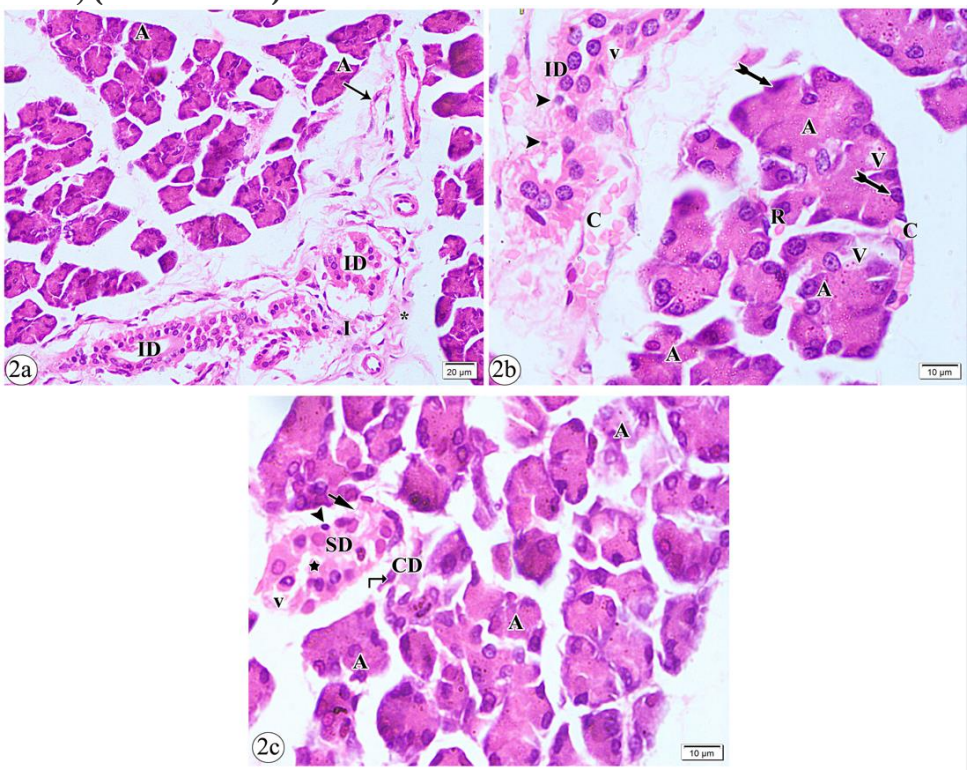

Fig.2: Photomicrographs of H&E-stained sections in the parotid gland in the tartrazine-treated group showing: **Fig. 2a:** The gland consists of lobules separated by thickened connective tissue septa (thin arrow) with interstitial cellular infiltration (I) and homogenous acidophilic material (*) The interlobular (ID)ducts appeared with disorganized cellular lining **(H & E X400). Fig. 2b:** The cellular lining of the interlobular duct (ID) appeared with vacuolated cytoplasm (v) and pyknotic nuclei (arrowhead). Note congested blood vessels(C). The acini (A) appeared disorganized with vacuolations of the cytoplasm (V) and darkly stained nuclei (tailed arrow). Red blood cells extravasation is observed (R) **(H & E X1000). Fig. 2c:** The intercalated duct (CD) has flattened disorganized cellular lining (kinked arrow). The lining cells of the striated duct (SD) showed loss of striations (short arrow) in addition to vacuolated cytoplasm (v) and pyknotic nuclei (arrowhead) with shedding of their epithelial lining into the lumen (star). Note disorganized acini (A) **(H & E X1000).**

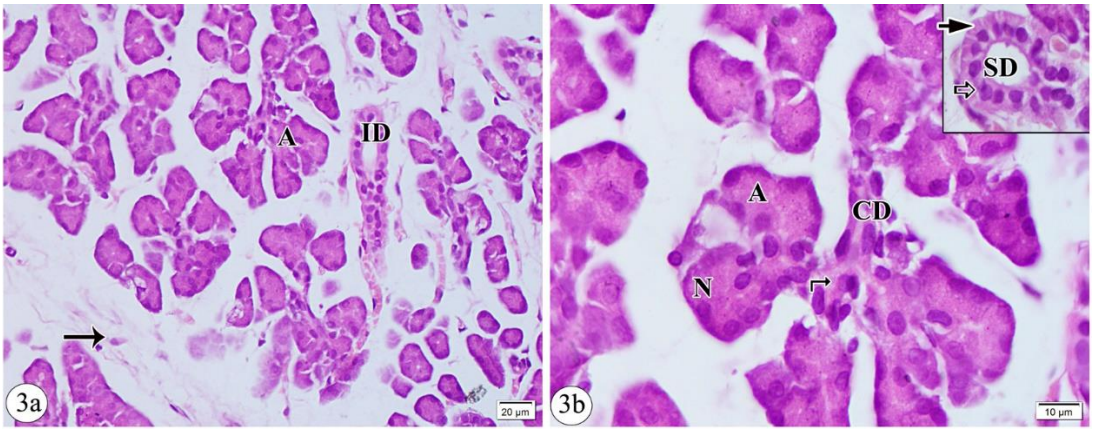

Fig.3: Photomicrographs of H & E-stained sections in the parotid gland in the tartrazine and omega-3 treated group showing**: Fig. 3a:** Parenchyma consists of lobules showing acini (A) separated by thin connective tissue septa (thin arrow). Interlobular duct appears with normal lining (ID) **(H & E X400). Fig. 3b:** Acini (A) are lined with pyramidal cells with vesicular nuclei (N). Intercalated duct (CD) appears branched with a low cuboidal lining (kinked arrow). **Inset:** The striated ducts (SD) appear relatively normal with basal striations (short arrow) and rounded central nucleus (thick arrow) **(H & E X1000).**

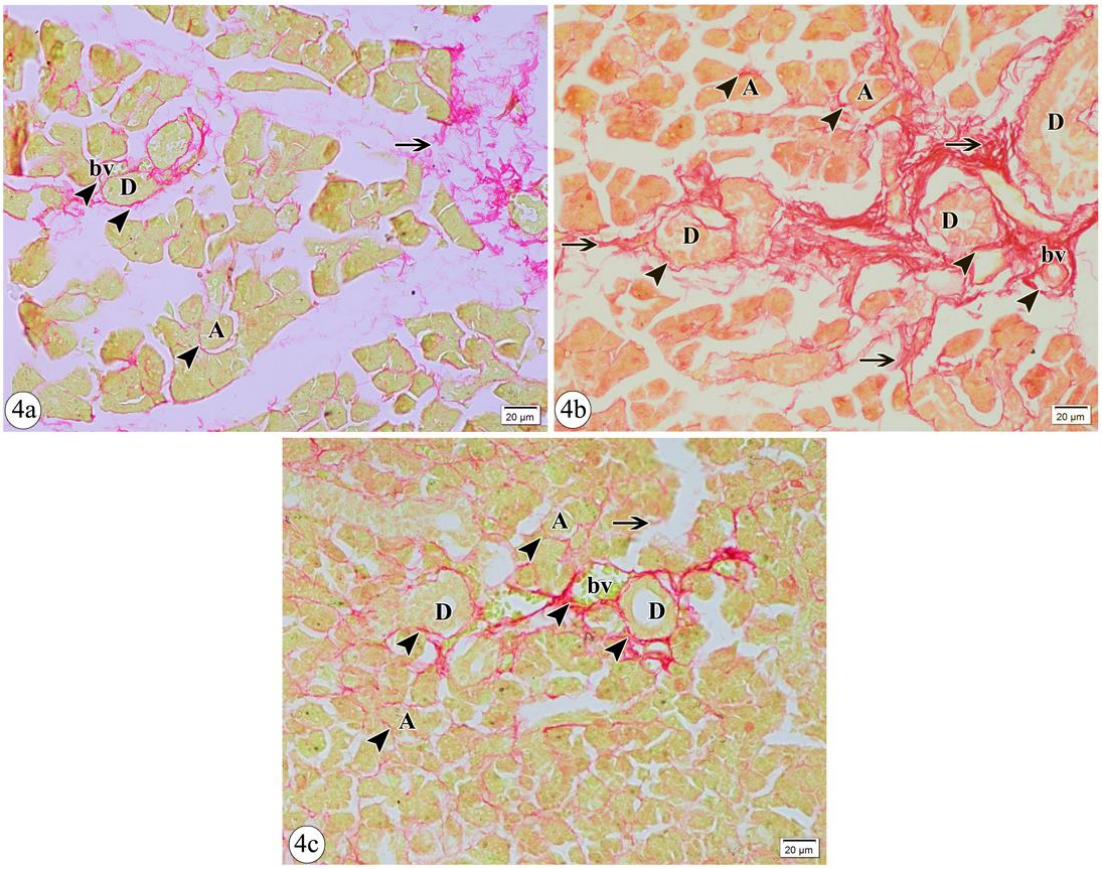

Fig. 4: Photomicrographs of Sirius red stained sections in the parotid gland in the control group (a), the tartrazine-treated group (b) and the tartrazine and omega-3 treated group (c) showing **Fig. 4a**: Fine collagen fibers (arrowhead) surrounding acini(A), the interlobular ducts (D) and blood vessels (bv) and in the interlobular septa(arrow). **Fig. 4b**: Intense collagen deposition (arrowhead) surrounding acini (A) and interlobular ducts (D) and its surrounding blood vessels (bv) and in the interlobular septa (arrow) **Fig. 4c:** Moderate amount of collagen fibers (arrowhead) surrounding ducts (D), acini (A) and blood vessels (bv) and in the interlobular septa(arrow) **(Sirius red X400)**

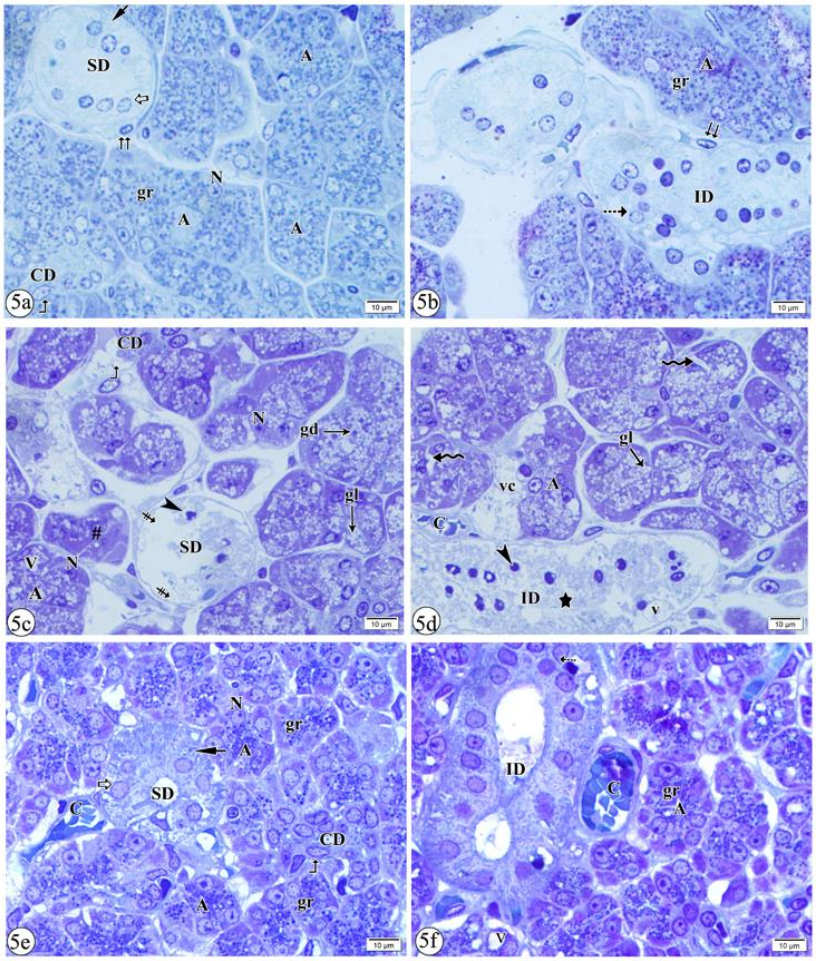

Fig. 5: Photomicrographs of semithin sections in the parotid gland in the control group (a-b), the tartrazine- treated group (c-d) and the tartrazine and omega-3 treated group(e-f) showing**:** **Fig. 5a:** Normal serous acini(A) lined by pyramidal cells with apical secretory granules of variable density (gr) and basal vesicular nuclei with prominent nucleoli (N). Intercalated duct (CD) in between the acini with low cuboidal lining cells with oval vesicular nuclei (kinked arrow). Striated ducts (SD) appear with a columnar cell lining with central rounded vesicular nuclei (thick arrow) and basally striated cytoplasm (short arrow) surrounded by myoepithelial cells with flattened nuclei (double arrow). **Fig. 5b:** Interlobular duct (ID) appeared with pseudostratified lining (dotted arrow) and surrounded by myoepithelial cells (double arrow). Note granules of different densities (gr) in acinar cells (A) **Fig. 5c:** The acinar cells cytoplasm showed vacuolations (V) and occupied by lightly stained granules (gl) with apparent decrease in densely stained granules (gd). Their nuclei are irregular and darkly stained (N). Note disorganized acini (#). The lining of intercalated ducts (CD) shows discontinuity and vacuolated cytoplasm (kinked arrow). Striated ducts (SD) lining cells show disruption (arrow with double stroke) with pyknotic nuclei (arrowhead), **Fig. 5d**: Interlobular duct (ID) lining cells appears with vacuolated cytoplasm (v) and pyknotic nuclei (arrowhead) and exfoliated cells in its lumen (star). Congested blood vessels (C) and marked vacuolations of the acinar cells (vc) are observed. Note the dilated intercellular spaces between acinar cells (wavy arrow) and the dominance of lightly stained granules (gl) **Fig. 5e:** Acinar cells (A) appear pyramidal in shape with rounded vesicular basal nuclei (N) and numerous granules of variable density (gr). Intercalated duct (CD) appears with low cuboidal lining cells and oval vesicular nuclei (kinked arrow). Striated ducts (SD) appear with a columnar cell lining with central rounded vesicular nuclei (thick arrow) and basal striations (short arrow). Some congested blood vessels are seen(C) **Fig.5f:** The interlobular ducts duct (ID) appeared with nearly normal pseudostratified lining (dotted arrow) and is surrounded by congested blood vessels (C). Note the variable density granules (gr) in acinar cells (A) and the presence of some vacuoles (V) **(Toluidine blue X1000)**.

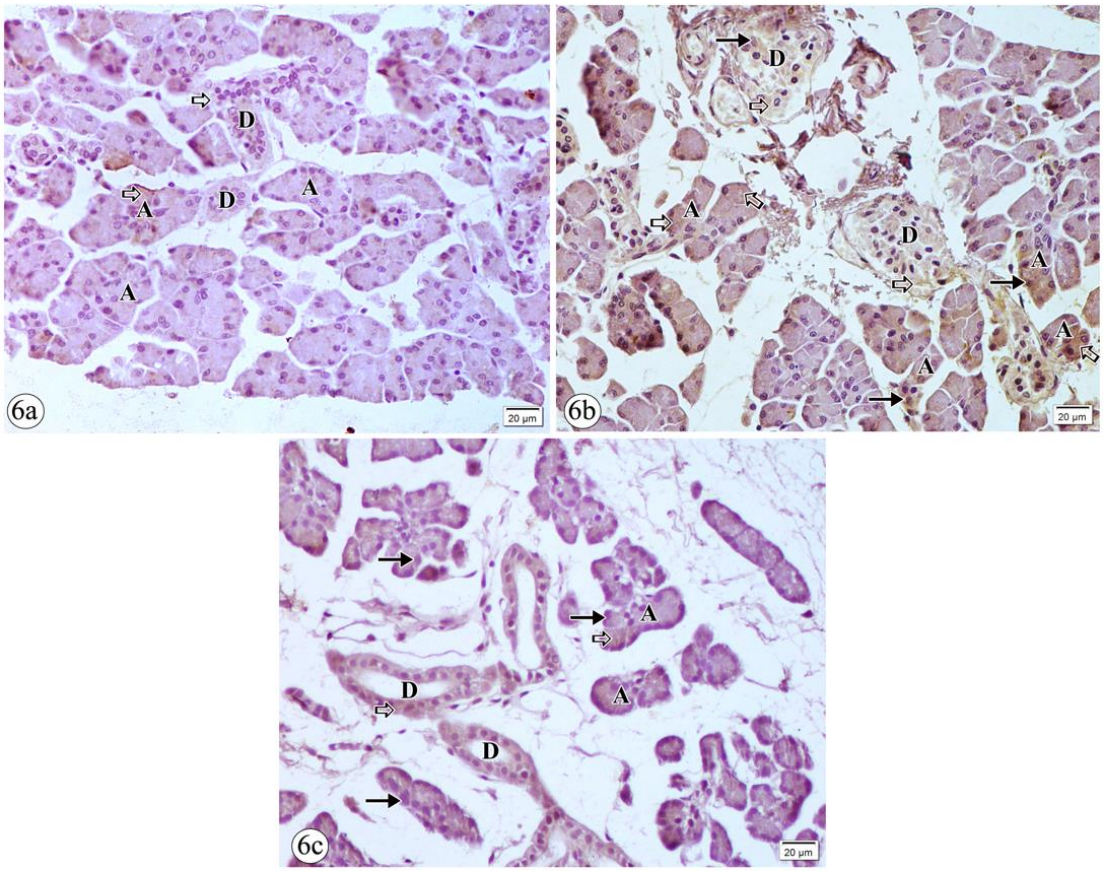

Fig. 6: Photomicrographs of the parotid gland in the control group (a), the tartrazine- treated group (b) and the tartrazine and omega-3 treated group (c) showing: **Fig. 6a:** Mild caspase-3 immunoexpression (arrow) in the acinar cells (A) and the duct epithelium (D). **Fig. 6b:** Strong caspase-3 immunoexpression in the nuclei (thin arrow) and cytoplasm (thick arrow) of the cells of acini (A) and the duct epithelium (D) is observed. **Fig. 6c**: Moderate caspase-3 immunoexpression (thick arrow) in the acinar cells (A) and in the duct lining cells (D) cytoplasm with most of nuclei show negative reaction (thin arrow). **(Caspase-3 immunostaining X400).**

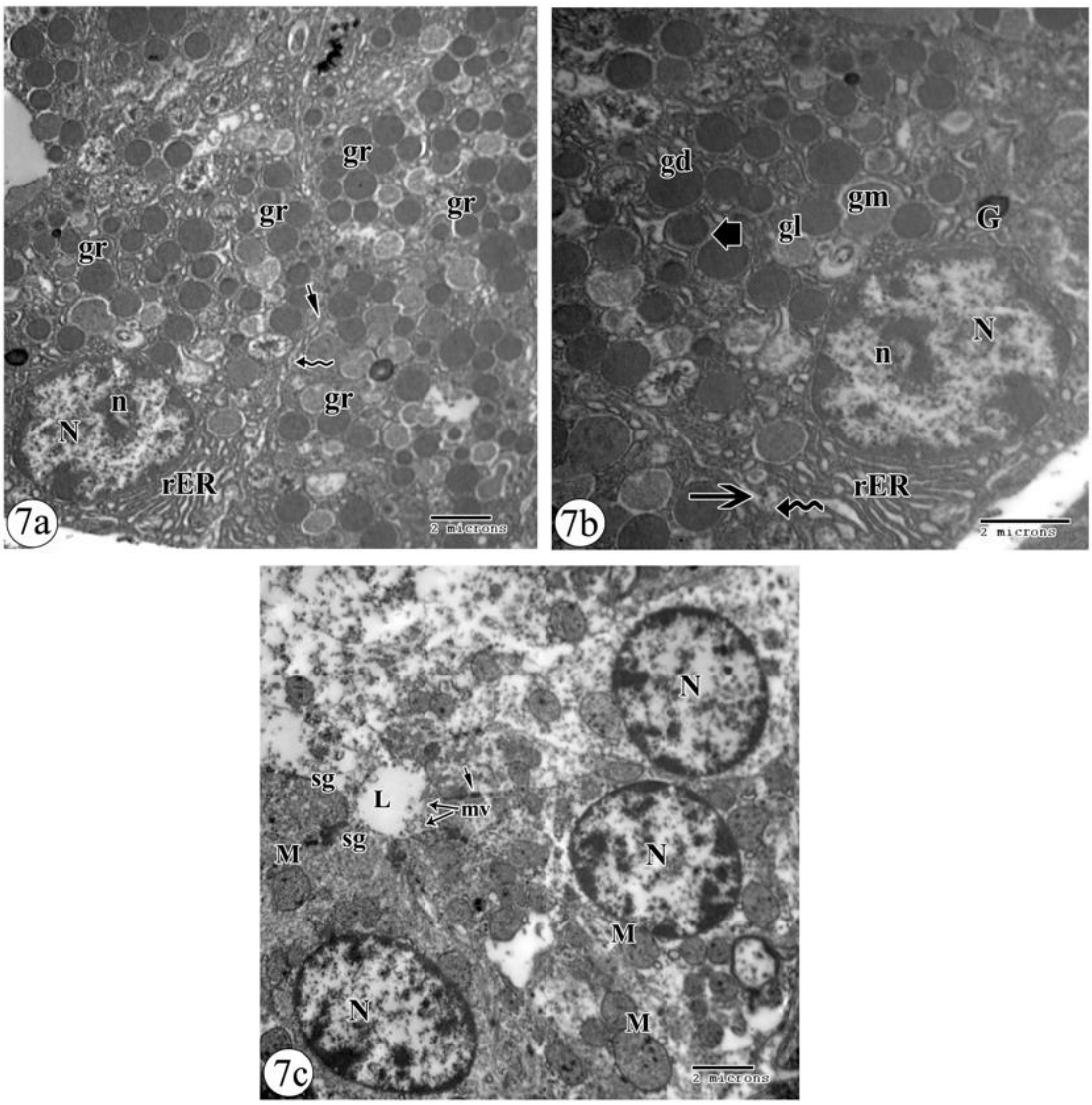

Fig. 7: Transmission electron photomicrographs of ultrathin sections in the parotid gland in the control group showing**: Fig. 7a:** Acinar cells appear pyramidal in shape with a basal rounded euchromatic nucleus (N) with well-defined nucleolus (n). Narrow intercellular space (wavy arrow) and intercellular junctional complexes (short arrow) are observed. The apical part of the cytoplasm shows a large number of secretory granules (gr) **(X4800). Fig. 7b**: A higher magnification showing that most of the secretory granules are of high electron density (gd) and some appear of moderate density (gm), others are of low density (gl). Note their well-defined membrane (thick arrow). Abundant rough endoplasmic reticulum cisternae (rER) are observed in addition to Golgi complex (G) Note the lateral infoldings of the plasma membrane (thin arrow) in the intercellular space (wavy arrow) **(X7200). Fig. 7c**: The lining columnar cells of the striated duct with rounded euchromatic central nucleus with regular nuclear membrane (N). The apical cytoplasm contains small secretory granules (SG). Mitochondria (M) are distributed in the basal and middle part of the cytoplasm. Note the presence of junctional complexes (short arrow) near the lumen (L) and the apical microvilli (mv) **(X4800).**

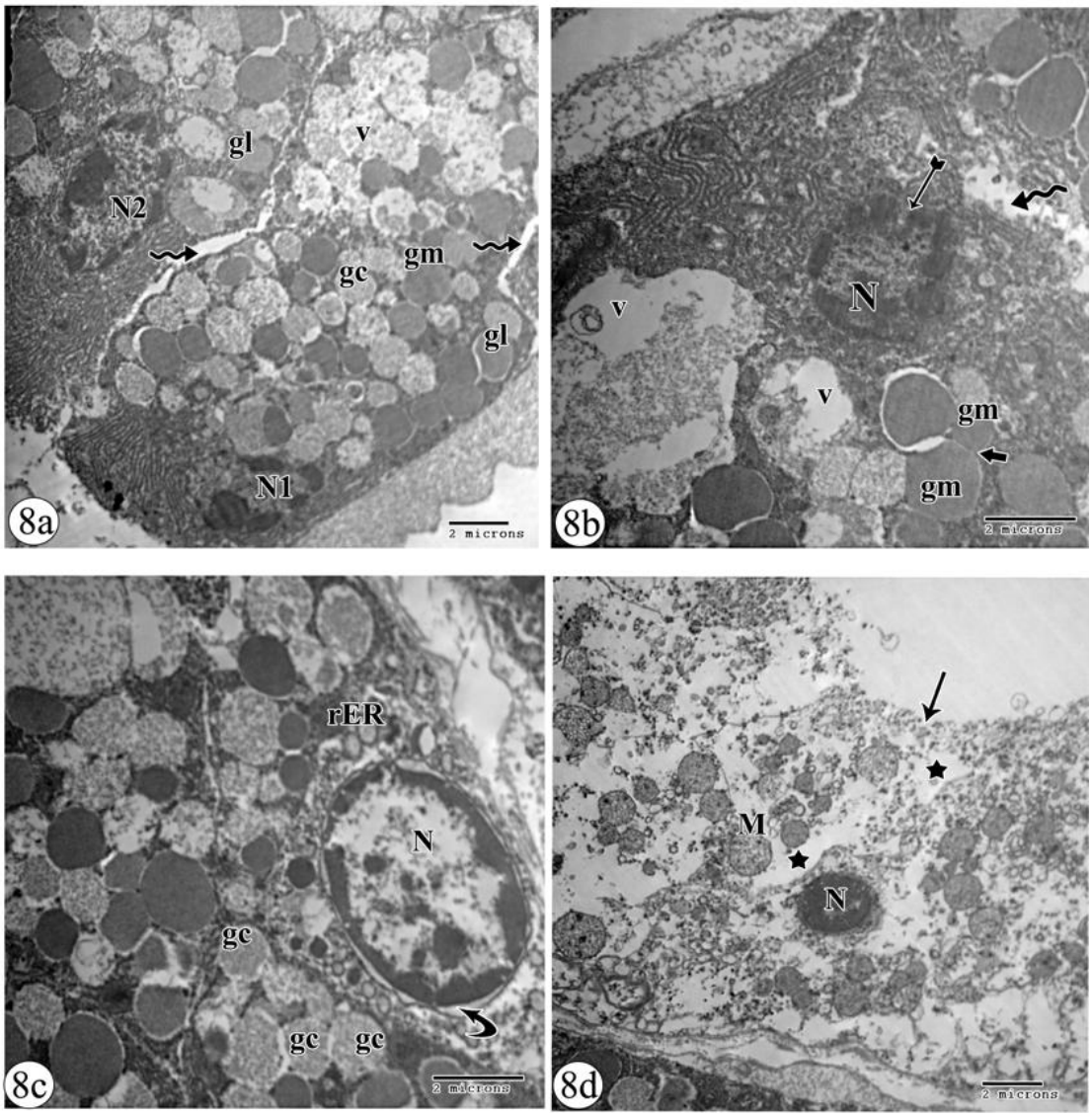

Fig. 8: Transmission electron photomicrographs of ultrathin sections in the parotid gland in the tartrazine- treated group showing**: Fig. 8a:** Acinar cells appear with irregular basal nuclei with condensed chromatin (N1) and (N2). The intercellular spaces appear dilated (wavy arrow) with absent junctional complexes. Some granules of moderate density (gm), of low electron density (gl) and numerous electron lucent granules (gc) were observed in the supranuclear region of the cytoplasm which encroach on the nucleus (N2) in addition to many vacuoles (v)**(X4800). Fig. 8b:** Acinar cell with indented nuclear membrane (tailed arrow) with a chromatin condensation (N). Note large vacuoles (v) and dilated intercellular canaliculi (wavy arrow). Granules of moderate electron density (gm) with fused outlines (thick arrow) are observed **(X7200). Fig. 8c:** Basal part of an acinar cell showing the nucleus with a peripherally condensed chromatin (N) and dilated perinuclear cisterna (curved arrow). Cystic dilatation of the rough endoplasmic reticulum (rER) cisternae is observed. Note numerous electron lucent granules with fused outlines (gc) **(X7200) Fig. 8d:** The lining columnar cells of the striated duct exhibits a condensed central nucleus (N) and rarified cytoplasm with loss of most of organelles (star). Mitochondria with destructed cristae are observed (M). Note absence of microvilli (arrow) **(X4800).**

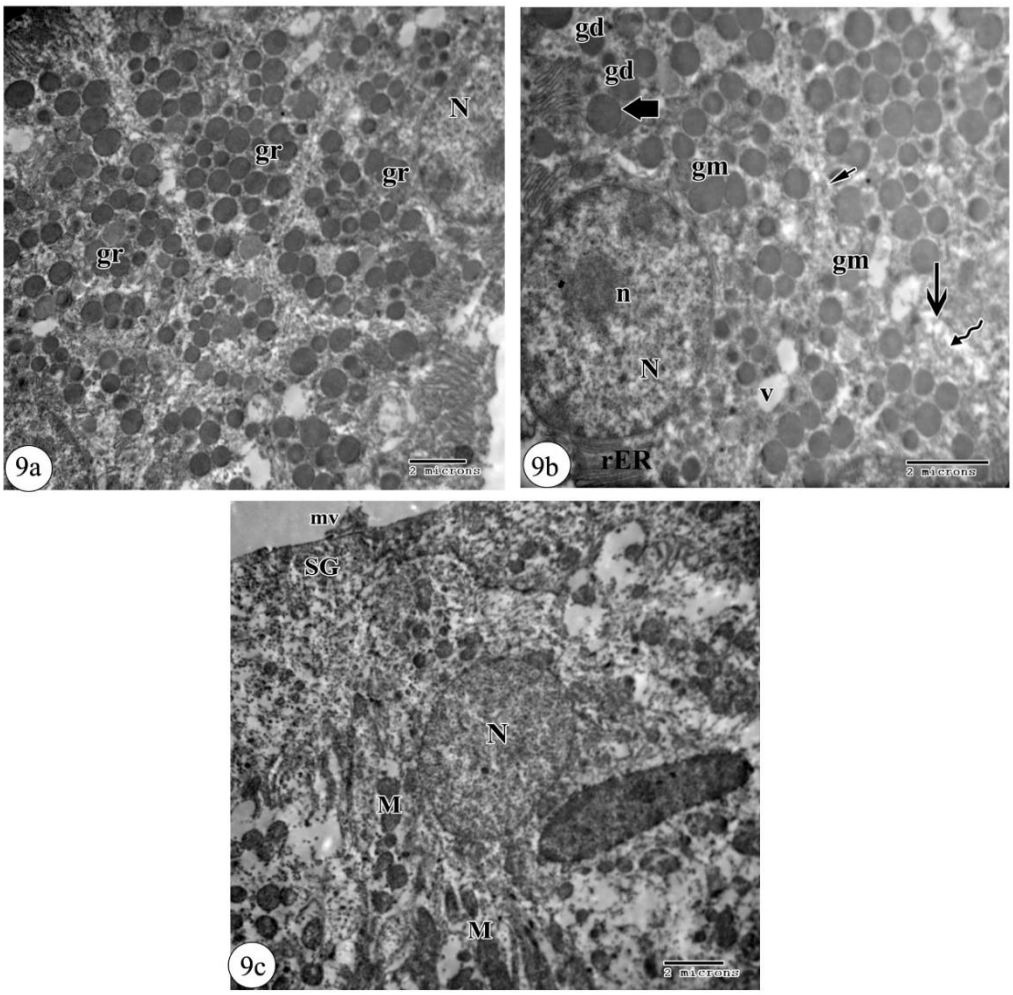

Fig. 9: Transmission electron photomicrographs of ultrathin sections in the parotid gland in the tartrazine and omega-3 treated group showing: **Fig. 9a:** Acinar cells appear pyramidal in shape with a basal nucleus (N). The cytoplasm shows a large number of secretory granules of different electron density in the apical part (gr) **(X4800). Fig. 9b**: The basal part of an acinar cell shows a basal euchromatic rounded nucleus (N) with a well-defined nucleolus (n). High electron dense granules(gd) and many granules of moderate density (gm) are observed with a defined membrane (thick arrow). Parallel cisternae of rough endoplasmic reticulum (rER) are observed basally. Note the lateral infoldings of the plasma membrane **(**long arrow) in intercellular canaliculi (wavy arrow), intercellular junctional complexes (short arrow) and the presence of some vacuoles (v) **(X7200). Fig. 9c**: The lining columnar cells of the striated duct with rounded central euchromatic nucleus with regular nuclear membrane (N). The apical cytoplasm contains small secretory granules (SG). The mitochondria (M) appear nearly normal and distributed longitudinally in the basal part. The apical microvilli (mv) are reserved **(X4800)**.

Table 1: Mean ± SE of the area percentage for the collagen fibers staining and caspase-3 immunostaining in the different experimental groups:

	Control group	**Tartrazine-treated group**	**Tartrazine and Omega 3 fatty acids treated group**
Area percentage of collage fibers staining	12.88± 0.49	24.12 ±0.74*	14.23±0.22#
Area percentage of caspase-3 immunostaining	8.32±0.46	27.65± 0.52*	11.89± 0.30#

***** Significant ($p < 0.05$) versus the control group.

\# Significant ($p < 0.05$) versus the tartrazine-treated group.

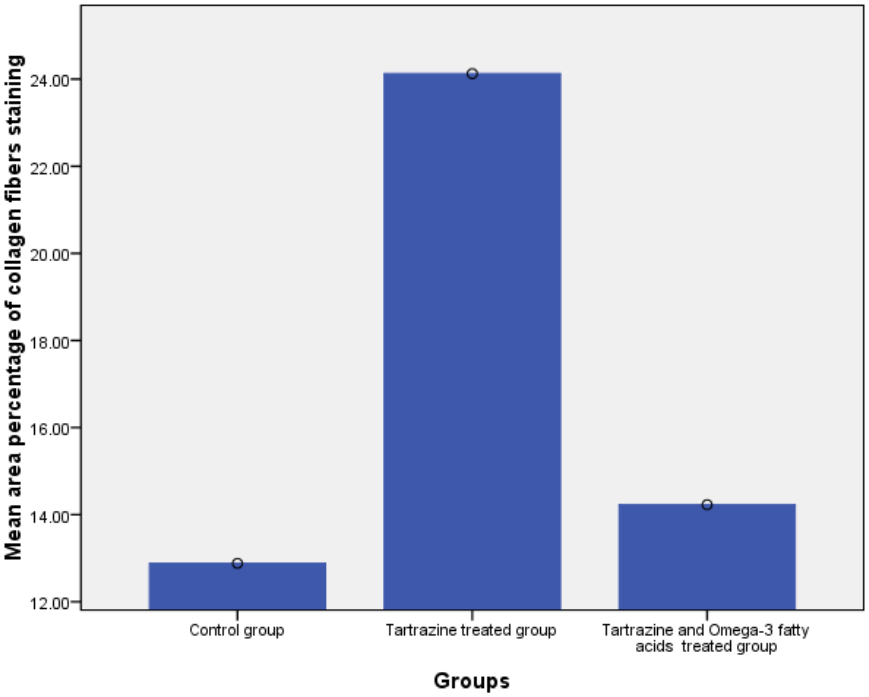

Graph 1: Comparison of the studied groups regarding the mean area percentage of the collagen fibers staining by Sirius red stain

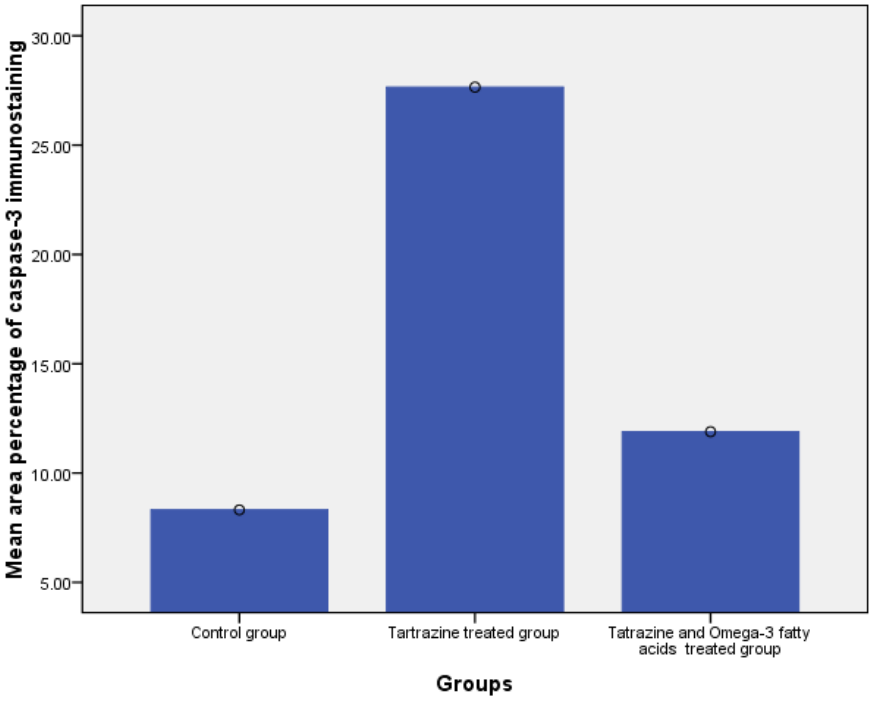

Graph 2: Comparison of the studied groups regarding the mean area percentage of caspase -3 immunostaining.

DISCUSSION

Tartrazine is one of the widely used food additives all over the world. Azo dyes have a significant consideration since they can cause health defects and exert threat to the gastrointestinal tract, kidney and the nervous system (Wopara *et al.*, 2021). The present study evaluated the ability of omega-3 fatty acids to improve the parotid gland pathological changes caused by tartrazine.

In the present study, the results showed that an oral administration of tartrazine to albino rats altered the histological structure of parotid gland. Abnormal dark-stained nuclei and numerous intracellular vacuoles in acinar cells were observed. These results are similar to the findings of El-Sakhawy *et al.* (2019) who carried out a study on the effect of tartrazine administration on the submandibular glands of adult male albino rats. They found that small vacuoles appeared inside the cytoplasm of the acinar cells, and the nuclei showed a hyperchromatism and an abnormal mitosis. The present findings were also in an agreement with Saxena & Sharma (2015) who indicated that tartrazine administration alters the histological structure of liver and kidney. Ruse *et al.* (2010) reported that tartrazine causes stasis, congestion and edema in the liver and the kidney of Guinea pigs that led to an apoptosis in the hepatocytes and renal atrophy.

Likewise, Ghonimi and Elbaz (2015) reported a diffuse degeneration, severe steatosis, necrosis of hepatic tissue as well as vacuolations in cerebellar neurons of Westar rats after the tartrazine exposure.

Azo dyes are catalyzed by peroxidases and azo reductases and produce semiquinone radicals and aromatic amines. Semiquinone radicals generate hydroxyl radicals, superoxide radicals and H_2O_2 that cause cellular defense weakening, consequently leading to a variety of oxidative stress-related disorders (Demirkol *et al.,* 2012). Tartrazine was documented to increase oxidative stress in the rats, by induction of an elevation in malondialdehyde as the end product of lipid peroxidation with reduction in glutathione level (Essawy *et al.*, 2022). Administration of tartrazine as well, decreased the activity of antioxidant enzymes (catalase, superoxide dismutase, and glutathione reductase) (Al-Seeni et al., 2018). Even though acceptable daily intake levels of food azo dyes were found by Bhatt *et al.* (2018) to adversely affect and alter biochemical markers of brain tissue and cause oxidative damage.

The present study revealed intense collagen fibers deposition around the acini, ducts and the congested blood vessels that was observed in the parotid tissue in the tartrazine-treated rats when compared to that of the control group and this was confirmed statistically. This was in accordance with Kandeel & Sharaf Eldin, (2021) who detected a significant increase in the amount of mucosal collagen fibers deposition in the jejunal mucosa in tartrazine treated rats. Oxidation products such as lipid peroxidation products stimulate expression of α-collagen and collagen synthesis and this could explain the presence of disorganized acini (Altayeb, 2018). Consistently these observations were in accordance with Essawy *et al.* (2022) who reported an elevation in the levels of TNF-α, IL-1β and IL-6 in the tartrazine -treated rat brain. TNF-α - inflammatory signals are released by the damaged tissue, stimulating the fibroblasts differentiation and consequently fibrosis (Limaye *et al.,* 2019).

Interstitial cellular infiltration and congested blood vessels were observed in the tartrazine treated parotid tissue. These findings are considered a part of the oxidative-inflammatory stress caused by tartrazine (Wopara *et al.,* 2021).

Toluidine blue-stained semithin sections examination indicated that most of the secretory granules of acinar cells were of low density that was confirmed on ultrastructural examination. According to Selim (2013) the dominance of electron-lucent secretory granules is a sign in the degenerated parotid gland. Maciejczyk *et al.* (2018) reported that a decrease in the salivary

flow occurred when the rats were subjected to an oxidative stress.

There was a significant increase in the tubular and acinar lining cells caspase- 3 immunostaining. This was similar to the results obtained by Abd-Elhakim *et al*. (2019) who reported a significant increase in the hepatic and renal immunoexpression of the caspase-3 in tartrazine-treated rats. Caspase-3 is considered as a main molecule in the apoptosis process (Poprac, *et al.*, 2017). These results could be due to the oxidative stress of tartrazine that activates ROS-mitochondria-Casp3-apoptosis cascades (Essawy *et al.*, 2022)

Ultrastructurally, the present results showed degenerative changes in the acinar cells in which condensation of chromatin, cystic dilatation of rough endoplasmic reticulum cisternae and cytoplasmic vacuolations were noticed. Similar findings were observed in the cells of the gastric mucosa in rats exposed to tartrazine (Elwan & Ibrahim 2019). Most of secretory granules in the acinar cells appeared electron lucent and some appeared with fused outlines. It was reported that reactive oxygen species attack the proteins and lipids that form the secretory granules membrane leading to its damage. In addition, they cause zymogen granules stability loss through an interaction with the protein contents and the nucleic acids of them (Hassan *et al.,* 2021). Similar observations were demonstrated by Nasr El-Din &Abdel Fattah (2020) in hypothyroid rats and they were attributed to an increase in the Bax/Bcl-2 ratio.

Dilated intercellular canaliculi were observed in semithin sections and was confirmed on ultrastructural examination. These findings could be attributed to reactive oxygen species release, that disturb the integrity of the plasma membrane and disrupt the intercellular junctions (EL-Sayed *et al.*, 2018). Nasr El-Din & Abdel Fattah, (2020) attributed the observed dilatation of the intercellular canaliculi in parotid gland acini to a dysfunction in the myoepithelial cells.

In the present study a degenerated cellular lining in the duct epithelium was observed in the form of degenerated mitochondria, rarified cytoplasm and pyknotic nuclei. Similar ultrastructural alterations were recorded in the hepatocytes and the epithelium of renal tubules in the rats treated with tartrazine (Khayyat *et al.*, 2017).

The present results suggested that the combination of omega-3 fatty acids with tartrazine could provide protection against the degenerative changes observed in the parotid gland of the tartrazine treated group. Histological examination of the parotid gland in the tartrazine and omega-3 group showed an almost normal histological appearance of cellular lining of the ducts and serous acini with a minimal cytoplasmic vacuolation. These findings are in accordance with Mohamed *et al.* (2015) who reported that Cod liver oil ,which is a rich source of omega-3 fatty acids, attenuated the structural changes in the brain of tartrazine-treated rats. These results could be explained by the antioxidant, anti-apoptotic and anti-inflammatory effects of omega-3 fatty acids (Mahmoud *et al.,* 2019). The present observations are in agreement with Elaziz & Laag (2018) who indicated the decrease in degenerative changes induced by bisphenol on the rat hippocampus on concomitant use of omega-3 fatty acids.

Previous studies have also described that omega-3 fatty acids had the capacity of increasing antioxidant enzymes activity and contributing to reduce ROS production (Yang *et al.,* 2019).

Omega-3 fatty acids, according to the present study, induce a statistically significant decrease in the collagen fibers deposition in parotid gland that was caused by tartrazine. This was in accordance with El Desouky *et al.*

(2019) who reported the ameliorative role of omega-3 fatty acids in the fibrosing effect of caffeine on the rat pancreas. The pancreas and parotid gland are known to have morphological and functional similarities (Tiffon, 2020). This observation could be explained by the fact that omega-3 produce a decrease in the production of TNF-a, IL-1b, IL- 6 and various growth factors by endotoxin-stimulated monocytes or mononuclear cells (Ellulu et al., 2015). Furthermore, omega-3 fatty acids reduce acute and chronic inflammatory reaction through various pathways (Koppelmann *et al.,* 2021).

In addition, the present immunohistochemical findings confirmed the protective effect of the co-administration of omega-3 fatty acids with tartrazine where a significant decrease in the area % of caspase-3 immunoexpression was detected in the omega-3 and tartrazine treated rats. These results were consistent with Saleh *et al.* (2022) who found that omega-3 fatty acids decreased the hepatic caspase-3 expression and the percentage of caspase-3 positive cells in doxorubicin intoxicated liver. This could be attributed to the anti-apoptotic effect of omega-3 fatty acids (Koppelmann *et al.,* 2021).

Conclusion and Recommendation:

Tartrazine has histological, ultrastructural and immunohistochemical degenerative effects on the rats' parotid gland acini and the duct system. The concomitant administration of omega-3 fatty acids helps in improving the histological picture and reducing these effects. The excessive use of tartrazine as a food additive should be minimized as much as possible.

Conflicts:

There are no conflicts of interest.

REFERENCES

Abad, A., & Shahidi, F. (2020). Compositional characteristics and oxidative stability of chia seed oil (Salvia hispanica L). *Food Production, Processing and Nutrition*, 2, 1–8.

Abd-Elhakim, Y. M., Moustafa, G. G., Hashem, M. M., Ali, H. A., Abo-EL-Sooud, K., & El-Metwally, A. E. (2019). Influence of the long-term exposure to tartrazine and chlorophyll on the fibrogenic signalling pathway in liver and kidney of rats: the expression patterns of collagen 1-α, TGFβ-1, fibronectin, and caspase-3 genes. *Environmental Science and Pollution Research*, *26*(12), 12368–12378. https://doi.org/10.1007/s11356-019-04734-w

Akkapinyo, C., Subannajui, K., Poo-Arporn, Y., & Poo-Arporn, R. P. (2021). Disposable electrochemical sensor for food colorants detection by reduced graphene oxide and methionine film modified screen printed carbon electrode. *Molecules*, *26*(8). https://doi.org/10. 3390/ molecules26082312

Al-Seeni, M. N., El Rabey, H. A., Al-Hamed, A. M., & Zamazami, M. A. (2018). Nigella sativa oil protects against tartrazine toxicity in male rats. *Toxicology Reports*, *5*, 146–155. https://doi.org/10.1016/ j. toxrep.2017.12.022

Altayeb, Z. (2018). Possible Protective Role of Green Tea Extract on Male Rat Parotid Gland in High Fat Diet Induced Obesity (Histological Study). *Journal of Medical Histology*, *2*(1), 69–80. https://doi.org/10.21608/ jmh. 2017. 1531. 1025

Amano, O., Mizobe, K., Bando, Y., & Sakiyama, K. (2012). Advance Publication Review Anatomy and Histology of Rodent and Human Major Salivary Glands-Overview of the Japan Salivary

Gland Society-Sponsored Workshop. *Acta Histochem. Cytochem*, *45*(5), 241–250. https://doi.org/10. 1267/ahc. 12013

Bancroft, JD & Layton C (2019). The hematoxylin and eosin In: Suvarna SK, Layton C and Bancroft JD, editors Bancroft's Theory and Practice of Histological Techniques, 8th Edition, Chapter 10, Elsevier Limited, 126-138.

Bhatt, D., Vyas, K., Singh, S., John, P. J., & Soni, I. (2018). Tartrazine induced neurobiochemical alterations in rat brain sub-regions. *Food and Chemical Toxicology*, *113*, 322–327. https://doi.org/10.1016/j.fct.20 18.02.011

Boussada, M., Lamine, J. A., Bini, I., Abidi, N., Lasrem, M., El-Fazaa, S., & El-Golli, N. (2017). Assessment of a sub-chronic consumption of tartrazine (E102) on sperm and oxidative stress features in Wistar rat. *International Food Research Journal*, *24*(4), 1473–1481.

Dawes, C., Pedersen, A. M. L., Villa, A., Ekström, J., Proctor, G. B., Vissink, A., Aframian, D., McGowan, R., Aliko, A., Narayana, N., Sia, Y. W., Joshi, R. K., Jensen, S. B., Kerr, A. R., & Wolff, A. (2015). The functions of human saliva: A review sponsored by the World Workshop on Oral Medicine VI. *Archives of Oral Biology*, *60*(6), 863–874. https://doi.org/ 10.1016/j. archoralbio. 2015. 03.004

Demirkol, O., Zhang, X., & Ercal, N. (2012). Oxidative effects of Tartrazine (CAS No. 1934-21-0) and New Coccin (CAS No. 2611-82-7) azo dyes on CHO cells. *Journal für Verbraucherschutz und Lebensmittelsicherheit*, *7*(3), 229-236.

El Desouky, A. A., Zaid, A. A., El Saify, G. H., & Noya, D. A. (2019). Ameliorative effect of omega-3 on energy drinks - Induced pancreatic toxicity in adult Male albino rats. *Egyptian Journal of Histology*, *42*(2), 324–334. https://doi.org/10. 21608/EJH.2019.47568

Elaziz, H. O. A., & Laag, E. M. (2018). Histological study of the possible protective action of omega-3-fatty acids on the injurious effect induced by Bisphenol A on rat hippocampus. *Egyptian Journal of Histology*, *41*(1), 39–54. https://doi.org/10. 21608/EJH.2018.7520

Ellulu, M. S., Khaza'ai, H., Abed, Y., Rahmat, A., Ismail, P., & Ranneh, Y. (2015). Role of fish oil in human health and possible mechanism to reduce the inflammation. *Inflammopharmacology*, *23*(2–3), 79–89. https://doi.org/10. 1007/s10787-015-0228-1

El-Sakhawy, M. A., Mohamed, D. W., & Ahmed, Y. H. (2019). Histological and immunohistochemical evaluation of the effect of tartrazine on the cerebellum, submandibular glands, and kidneys of adult male albino rats. *Environmental science and pollution research international*, *26*(10), 9574–9584. https://doi.org/10.1007/ s11356-019-04399-5

EL-Sayed,S. K., Abo El-Yazed A. A., EL-Bakary, N.A. and EL-BAKARY R. H. (2018). Histological and Immunohistochemical Study of the Effect of Alendronate on the Submandibular Salivary Gland

of Adult Male Albino Rat and the Possible Protective Effect of Propolis. *The Medical Journal of Cairo University*, *86*(9), 3119–3132. https://doi.org/10.21608/mjcu.2018.59886

Elwan, W., Ibrahim, M. (2019). Effect of tartrazine on gastric mucosa and the possible role of recovery with or without riboflavin in adult male albino rat. *Egyptian Journal of Histology*, 42(2), 297-311. doi: 10.21608/ejh.2019.6312.1043

Engel, F., Pinto, L. H., Del Ciampo, L. F., Lorenzi, L., Heyder, C. D., Häder, D. P., & Erzinger, G. S. (2015). Comparative toxicity of physiological and biochemical parameters in Euglena gracilis to short-term exposure to potassium sorbate. Ecotoxicology (London, England), 24(1), 153–162.

Essawy, A. E., Mohamed, A. I., Ali, R. G., Ali, A. M., & Abdou, H. M. (2022). Analysis of Melatonin-Modulating Effects Against Tartrazine- Induced Neurotoxicity in Male Rats: Biochemical, Pathological and Immunohistochemical Markers. *Neurochemical Research*,. https://doi.org/10.1007/s11064-022-03723-9

Fortea, J. I., Fernández-Mena, C., Puerto, M., Ripoll, C., Almagro, J., Bañares, J., Bellón, J. M., Bañares, R., & Vaquero, J. (2018). Comparison of Two Protocols of Carbon Tetrachloride-Induced Cirrhosis in Rats - Improving Yield and Reproducibility. *Scientific Reports*, *8*(1), 1–10. https://doi.org/ 10.1038/s41598-018-27427-9

Galal, M. K., Elleithy, E. M. M., Abdrabou, M. I., Yasin, N. A. E., & Shaheen, Y. M. (2019). Modulation of caspase-3 gene expression and protective effects of garlic and spirulina against CNS neurotoxicity induced by lead exposure in male rats. *NeuroToxicology*, *72*, 15–28. https://doi.org/10.1016/j. neuro. 2019.01.006

Ghonimi WA and Elbaz A: (2015) Histological changes of selected Westar rat tissues following the ingestion of tartrazine with special emphasis on the protective effect of royal jelly and cod liver oil. *Journal of cytology & histology*, 6(4): 1-6

Harrison, J. D. (2021). Salivary Gland Histology. In *Surgery of the Salivary Glands*. Robert L. Witt, Elsevier Inc. Pages 37-42 https://doi.org/10.1016/b978-0-323-67236-8.00005-5

Hassan, E., Adawy, H., & Rabea, A. (2021). Histological, Fluorescence and Ultrastructural Assessment of Presumptive Effect of Carbimazole Treatment and its Co-administration with Bone Marrow-Derived Mesenchymal Stem Cells on Parotid Glands of Albino Rats. *Egyptian Journal of Histology*, *45*(2), 619-639. https://doi.org/10.21608/ejh.2021.71830.1460

Humphrey, S.P., Williamson, R.T., 2001. A review of saliva: normal composition, flow, and function. *The Journal of prosthetic dentistry*, 85 (2), 162–169. https://doi.org/10.1067/mpr.2001.113778

Iheanyichukwu, W., Adegoke, A. O., Adebayo, O. G., Emmanuel U, M., Egelege, A. P., Gona, J. T., & Orluwene, F. M. (2021). Combine Colorants of Tartrazine and Erythrosine induce kidney injury:

involvement of TNF-α gene, Caspase-9 and KIM-1 gene expression and kidney function indices. *Toxicology Mechanisms and Methods*,31 (1), 67–72.

Junqueira, L.C., Bignolas, G., Brentani, R.R. (1979). Picrosirius staining plus polarization microscopy, a specific method for collagen detection in tissue sections. *The Histochemical journal*, 11 (4), 447–4455.

Kandeel, S., & Sharaf Eldin, H. E. M. (2021). The possible ameliorative effect of manuka honey on tartrazine induced injury of the jejunal mucosa with the role of oxidative stress and TNF-alpha: Histological and morphometric study. *Egyptian Journal of Histology*, *44*(1), 48–60. https://doi.org/ 10.21608/ EJH.2020.28580. 1280

Khayyat, L., Essawy, A., Sorour, J., & Soffar, A. (2017). Tartrazine induces structural and functional aberrations and genotoxic effects in vivo. *PeerJ*., *2017*(2), 1–14. https:// doi.org/10.7717/peerj.3041

Koppelmann, T., Pollak, Y., Ben-Shahar, Y., Gorelik, G., & Sukhotnik, I. (2021). The mechanisms of the anti-inflammatory and anti-apoptotic effects of omega-3 polyunsaturated fatty acids during methotrexate-induced intestinal damage in cell line and in a rat model. *Nutrients*, *13*(3), 1–15. https://doi.org/10. 3390/nu13030888

Limaye, A., Hall, B. E., Zhang, L., Cho, A., Prochazkova, M., Zheng, C., Walker, M., Adewusi, F., Burbelo, P. D., Sun, Z. J., Ambudkar, I. S., Dolan, J. C., Schmidt, B. L., & Kulkarni, A. B. (2019). Targeted TNF-α Overexpression Drives Salivary Gland Inflammation. *Journal of Dental Research*, *98*(6), 713–719. https://doi.org/ 10.1177/0022034519837240

Maciejczyk, M., Matczuk, J., Żendzian-Piotrowska, M., Niklińska, W., Fejfer, K., Szarmach, I., Ładny, J. R., Zieniewska, I., & Zalewska, A. (2018). Eight-Week Consumption of High-Sucrose Diet Has a Pro-Oxidant Effect and Alters the Function of the Salivary Glands of Rats. *Nutrients*, *10*(10), 1530. https://doi.org/10.3390/nu1010 1530

Mahmoud, A. M., Nor-Eldin, E. K., & Elsayed, H. M. (2019). The possible protective effect of Omega 3 fatty acids against Bisphenol A induced disruption of pituitary-testicular axis in albino rat. Biohemical, Histological and Immunohistochemical study. *Egyptian Journal of Histology*, *42*(1), 215–228. https://doi.org/ 10.21608/ejh.2018.5474.1030

Meital, L. T., Windsor, M. T., Perissiou, M., Schulze, K., Magee, R., Kuballa, A., Golledge, J., Bailey, T. G., Askew, C. D., & Russell, F. D. (2019). Omega-3 fatty acids decrease oxidative stress and inflammation in macrophages from patients with small abdominal aortic aneurysm. *Scientific Reports*, *9*(1), 1–11. https://doi.org/10. 1038/s41598-019-49362-z

Mohamed, A. A. R., Galal, A. A. A., & Elewa, Y. H. A. (2015). Comparative protective effects of royal jelly and cod liver oil against neurotoxic impact of tartrazine on male rat pups brain. *Acta Histochemica*, *117*(7), 649–658. https://doi. org/10.1016/j.acthis.2015.07.0 02

Nasr El-Din, W. A., & Abdel Fattah, I. O. (2020). Histopathological and biochemical alterations of the parotid gland induced by experimental hypothyroidism in adult male rats and the possible therapeutic effect of Nigella sativa oil. *Tissue and Cell*, *65*(March), 101366. https://doi.org/10.1016/j.tice.2020.101366

Pogacean, F., Rosu, M. C., Coros, M., Magerusan, L., Moldovan, M., Sarosi, C., ... & Pruneanu, S. (2018). Graphene/TiO2-Ag based composites used as sensitive electrode materials for amaranth electrochemical detection and degradation. *Journal of the Electrochemical Society*, *165*(8), B3054.

Poprac, P., Jomova, K., Simunkova, M., Kollar, V., Rhodes, C. J., & Valko, M. (2017). Targeting Free Radicals in Oxidative Stress-Related Human Diseases. *Trends in pharmacological sciences*, *38*(7), 592–607. https://doi.org/10.1016/j. tips.2017.04.005

Roa, I., & Del Sol, M. (2019). Parotid gland comparative microscopic anatomy. *International Journal of Morphology*, *37*(2), 701–705. https://doi.org/10. 4067/S0717-95022019000200701

Rus, V., Gherman, C., Miclăuş, V., Mihalca, A., & Nadăş, G. C. (2010). Comparative toxicity of food dyes on liver and kidney in guinea pigs: A histopathological study. *Annals of the Romanian Society for Cell Biology*, *15*(1), 161-165.

Saleh, D. O., Mahmoud, S. S., Hassan, A., & Sanad, E. F. (2022). Doxorubicin-induced hepatic toxicity in rats: Mechanistic protective role of Omega-3 fatty acids through Nrf2/HO-1 activation and PI3K/Akt/GSK-3β axis modulation. *Saudi Journal of Biological Sciences*, *29*(7), 103308. https://doi.org/10. 1016/j.sjbs.2022.103308

Sanderson, T., Wild, G., Cull, A. M., Marston, J., & Zardin, G. (2019). Immunohistochemical and immunofluorescent techniques. In: Suvarna SK, Layton C and Bancroft JD, editors. Bancroft's Theory and Practice of Histological Techniques. 8th edition, Chapter 19, Elsevier Limited, Philadelphia.337–394.

Saxena, B., & Sharma, S. (2015). Food Color Induced Hepatotoxicity in Swiss Albino Rats, Rattus norvegicus. *Toxicology international*, 22(1), 152–157. https://doi.org/10.4103/0971-6580.172286

Selim, S.A. (2013). The effect of high-fat diet-induced obesity on the parotid gland of adult male albino rats: histological and immunohistochemical study. *The Egyptian Journal of Histology*, 36 (4): 772–780.

Tiffon, C. (2020). Defining parallels between the salivary glands and pancreas to better understand pancreatic carcinogenesis. *Biomedicines*, *8*(6).178. https://doi.org/10.3390/BIOMEDICINES8060178

Unda, S. R., Villegas, E. A., Toledo, M. E., Asis Onell, G., & Laino, C. H. (2020). Beneficial effects of fish oil enriched in omega-3 fatty acids on the development and maintenance of neuropathic pain. *Journal of Pharmacy and Pharmacology*, 72, 437–447.

Woods, A. E. and Stirling, J. W. (2019). Transmission electron microscopy. In: Suvarna SK, Layton C, Bancroft JD, editors. Theory and Practical Histological Techniques. 8th edition, Chapter 21, Churchill

Livingstone, Philadelphia. pp. 434-475.

Wopara, I., Modo, E. U., Adebayo, O. G., Mobisson, S. K., Nwigwe, J. O., Ogbu, P. I., Nwankwo, V. U., & Ejeawa, C. U. (2021). Anxiogenic and memory impairment effect of food color exposure: upregulation of oxido- neuroinflammatory markers and acetyl-cholinestrase activity in the prefrontal cortex and hippocampus. *Heliyon*, 7(3), e06378.

Yang, J., Fernández-Galilea, M., Martínez-Fernández, L., González-Muniesa, P., Pérez-Chávez, A., Martínez, J. A., & Moreno-Aliaga, M. J. (2019). Oxidative Stress and Non-Alcoholic Fatty Liver Disease: Effects of Omega-3 Fatty Acid Supplementation. *Nutrients*, *11* (4), 872. https://doi.org/10.3390/nu11040872

Zingue, S., Mindang, E. L. N., Awounfack, F. C., Kalgonbe, A. Y., Kada, M. M., Njamen, D., & Ndinteh, D. T. (2021). Oral administration of tartrazine (E102) accelerates the incidence and the development of 7,12-dimethylbenz(a) anthracene (DMBA)-induced breast cancer in rats. *BMC Complementary Medicine and Therapies*, *21*(1), 1–11. https://doi.org/10.1186/s12906-021-03490-0